

General Disclaimer

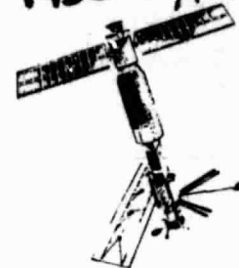
One or more of the Following Statements may affect this Document

- This document has been reproduced from the best copy furnished by the organizational source. It is being released in the interest of making available as much information as possible.
- This document may contain data, which exceeds the sheet parameters. It was furnished in this condition by the organizational source and is the best copy available.
- This document may contain tone-on-tone or color graphs, charts and/or pictures, which have been reproduced in black and white.
- This document is paginated as submitted by the original source.
- Portions of this document are not fully legible due to the historical nature of some of the material. However, it is the best reproduction available from the original submission.

157800-1-F

"Made available under NASA sponsorship
in the interest of early and wide dis-
semination of Earth Resources Survey
Program information and without liability
for any use made thereon."

9950-712



Informal Information Report

E83-10037

CR-16 9509

EVALUATION OF ERIM OPTICALLY PROCESSED SEASAT SAR DATA

D.R. LYZENGA, A. KLOOSTER Jr., J. MARKS,
and R.A. SHUCHMAN

Radar and Optics Division

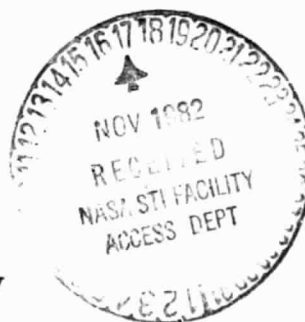
APRIL 1982

(E83-10037) EVALUATION OF ERIM OPTICALLY
PROCESSED SEASAT SAR DATA Informal
Information Report, Aug. 1981 - Apr. 1982
(Environmental Research Inst. of Michigan)
45 p HC A03/MF A01

N83-13531

Unclas
00037

CSCI 05B G3/43



Jet Propulsion Laboratory
California Institute of Technology
4800 Oak Grove Drive
Pasadena, California 91103

Contract No. 956105 (PRIME NAS7-100)
Technical Monitor: Dr. Daniel Held

ENVIRONMENTAL
RESEARCH INSTITUTE OF MICHIGAN
BOX 8618 • ANN ARBOR • MICHIGAN 48107

ORIGINAL PAGE 13
OF POOR QUALITY

Unclassified

SECURITY CLASSIFICATION OF THIS PAGE (When Data Entered)

REPORT DOCUMENTATION PAGE		READ INSTRUCTIONS BEFORE COMPLETING FORM
1. REPORT NUMBER 157800-1-F	2. GOVT ACCESSION NO.	3. RECIPIENT'S CATALOG NUMBER
4. TITLE (and Subtitle) EVALUATION OF ERIM OPTICALLY PROCESSED SEASAT SAR DATA		5. TYPE OF REPORT & PERIOD COVERED Informal Information Rpt. August 1981 - April 1982
		6. PERFORMING ORG REPORT NUMBER 157800-1-F
7. AUTHOR(s) D.R. Lyzenga, A. Klooster Jr., J. Marks, and R.A. Shuchman		8. CONTRACT OR GRANT NUMBER (s) 956105 (PRIME NAS7-100)
9. PERFORMING ORGANIZATION NAME AND ADDRESS Environmental Research Institute of Michigan Radar and Optics Division P.O. Box 8618; Ann Arbor, MI 48107		10. PROGRAM ELEMENT, PROJECT, TASK AREA & WORK UNIT NUMBERS
11. CONTROLLING OFFICE NAME AND ADDRESS Jet Propulsion Laboratory California Institute of Technology 4800 Oak Grove Drive; Pasadena, CA 91103		12. REPORT DATE April 1982
		13. NUMBER OF PAGES
14. MONITORING AGENCY NAME AND ADDRESS (if different from Controlling Office)		15. SECURITY CLASS. (of this report) Unclassified
		15a. DECLASSIFICATION/DOWNGRADING SCHEDULE
16. DISTRIBUTION STATEMENT (of this Report) Distribution of this report is unlimited.		
17. DISTRIBUTION STATEMENT (of the abstract entered in Block 20, if different from Report) Original photography may be purchased from EROS Data Center Sioux Falls, SD 57198		
18. SUPPLEMENTARY NOTES The technical monitor for this report was Dr. Daniel Held of the Jet Propulsion Laboratory.		
19. KEY WORDS (Continue on reverse side if necessary and identify by block number) Seasat SAR Radiometric calibration Image scale Doppler shift		
20. ABSTRACT (Continue on reverse side if necessary and identify by block number) This report summarizes the results of three studies on the radiometric and geometric properties of optically processed Seasat SAR imagery. The first study was performed to evaluate the accuracy with which the image scale can be pre- dicted based upon a knowledge of the SAR platform and recording system para- meters and the processor characteristics. The second study deals with the considerations involved in making radiometric measurements from image films, (continued)		

Unclassified

SECURITY CLASSIFICATION OF THIS PAGE (When Data Entered)

20. ABSTRACT (concluded)

including the use of point targets for calibration. The third study evaluates the effects of Doppler spectrum shifts on the radiometric calibration of the SAR image data over extended swath lengths.

Unclassified

SECURITY CLASSIFICATION OF THIS PAGE (When Data Entered)

PREFACE

The work described in this report was conducted by the Radar and Optics Division of the Environmental Research Institute of Michigan (ERIM). The work was supported by the Jet Propulsion Laboratory (JPL) Contract No. 956105, a subcontract under JPL's prime NASA contract NAS7-100. The report summarizes the entire contract performance period of August 1981 to April 1982. The JPL technical monitor for this report was Dr. Daniel Held.

This report discusses only Task II of the contract. Task I, which was concerned with a technical review of the JPL User's manual for the Seasat SAR Data, has been completed and sent to Dr. D. Held under separate cover.

Co-principal investigators for this program were Drs. Robert Shuchman and David Lyzenga. Mr. James Marks contributed the section on Image Scale Factors for ERIM-generated SEASAT SAR imagery. Mr. Alex Klooster performed the analysis on image film radiometric measurements, and Dr. D. Lyzenga carried out the study on radiometric effects of Doppler spectrum variations.

ACKNOWLEDGMENTS

It is a pleasure to acknowledge the aid of the following individuals in this study: Daniel Held and Benjamin Holt, for providing sensor data records for the Seasat orbits studied; a number of ERIM personnel were involved in generating this report including Jack Losee and Wally Kerce who optically processed the data, Charles Liskow who evaluated the geometric accuracy of the data, Liza Feezell who prepared the figures, and Barbara Burns and Richard Larson who reviewed this report.

PRECEDING PAGE BLANK NOT FILMED

TABLE OF CONTENTS

PREFACE	iii
ACKNOWLEDGMENTS	v
LIST OF FIGURES	ix
LIST OF TABLES	xi
1. INTRODUCTION	1
2. IMAGE SCALE DETERMINATION	3
2.1 Processing Method	
2.2 Evaluation	
2.3 Summary	
3. IMAGE FILM RADIOMETRY	11
3.1 Background	
3.2 Radar Cross Section Measurements	
3.3 Image Point Density Measurements	
3.3 Distributed Reflectance Measurements	
3.4 Summary and Recommendations	
4. RADIOMETRIC EFFECTS OF DOPPLER SPECTRUM VARIATIONS	25
4.1 Background	
4.2 Doppler Spectrum Measurements	
4.3 Radiometric Effects	
4.4 Summary	
REFERENCES	41

PRECEDING PAGE BLANK NOT FILMED

LIST OF FIGURES

1. Portion of Rev. 651 Image Used For Scale Evaluation	7
2. Typical Density vs. Exposure Plot For Photographic Film . . .14	
3. Effective Film "Gamma" For Points Not On The Linear Part Of The Curve	14
4. Response Curves For Point Targets And Step Wedges Using Kodak 3414 Film	20
5. Film Characteristics For Distributed Targets	21
6. Measured Doppler Spectrum For Area A	27
7. Measured Doppler Spectrum For Area B	27
8. Measured Doppler Spectrum For Area C	27
9. Measured Doppler Spectrum For Area D	27
10. Measured Doppler Spectrum For Area E	27
11. Corrected Doppler Spectrum For Area A, Rev. 757	29
12. Corrected Doppler Spectrum For Area B, Rev. 757	29
13. Corrected Doppler Spectrum For Area C, Rev. 757	29
14. Corrected Doppler Spectrum For Area D, Rev. 757	30
15. Corrected Doppler Spectrum For Area E, Rev. 757	30
16. Seasat Orbital Parameters And Associated Doppler Shifts For Rev. 757	32
17. Calculated Doppler Shifts Due To Earth Rotation And Spacecraft Attitude Changes, And Observed Peak Frequencies For Seasat Rev. 757	33
18. Ratio Of Output To Input Power Within A Frequency Interval Of 900 Hz Centered At The Doppler Peak Frequency	35

LIST OF FIGURES
(concluded)

19.	Ratio Of Output To Input Power For A Segment Of Rev. 757, Using A Frequency-Plane Aperture of 900 Hz Width Centered At The Actual Doppler Peak Frequency	36
20.	Ratio Of Output To Input Power For A Frequency Interval From -PRF To +PRF Versus Doppler Peak Frequency	37
21.	Ratio Of Output To Input Power For A Segment Of Rev. 757, Using A Frequency-Plane Aperture From -PRF To +PRF	38

LIST OF TABLES

1. SDR Data For Portion Of Rev. 651 Considered	5
2. Observed Differences In Across-Track Scale Factors Between SAR Image And Map	8
3. Corner Reflector Image Density Measurements	18
4. Doppler Peak Frequencies Measured For Rev. 757	31

EVALUATION OF OPTICALLY PROCESSED
SEASAT SAR DATA1
INTRODUCTION

This informal information report describes the results of three experiments which were performed to evaluate some of the characteristics of ERIM optically processed Seasat SAR data. Two previously reported engineering studies (Shuchman, et al., 1978, 1981) have evaluated various aspects of the Seasat SAR system and its products, including more detailed analyses of the data collection and recording systems, the image quality, and system radiometric effects.

The first experiment performed during the present study was intended to determine how accurately the scale of an optically processed image could be predicted using only the data recorded on the signal film and the information provided on the auxiliary data listing for the Seasat orbit considered. A set of images was made for a portion of Rev. 651 with a calculated scale of 1:250,000 and the results were compared with standard topographic maps to determine the actual scale of the images.

The second study dealt with the practical considerations involved in making radiometric measurements from Seasat image films. The feasibility of using calibrated point targets, i.e., corner reflectors, to measure the radar cross section of distributed scenes is evaluated and recommendations are made to improve the accuracy of this procedure.

The third study explored the radiometric effects of Doppler spectrum variations due to earth rotation and spacecraft altitude changes. These effects are calculated and compared with measurements using data from Seasat Rev. 757, and possible correction procedures are discussed. The results of this study are especially relevant to the interpretation of data contained in long swaths of Seasat imagery.

2
IMAGE SCALE DETERMINATION

This study was a test of the accuracy with which the scale of a given Seasat image can be predicted using only the system parameters contained in the Sensor Data Record (SDR), the properties of the film recording system as inferred from an examination of the signal film, and the magnification settings of the optical processor. The study was carried out by setting up the optical processor so that output imagery with a nominal scale of 1:250,000 was produced and then comparing this imagery with a 1:250,000 scale map. This section of the report describes the method used to determine the processor settings and the results of the scale comparisons.

2.1 PROCESSING METHOD

The data used in this study were collected during Seasat Rev. 651 near Louisville, Kentucky. The data were read from High Density Digital Tape (HDDT) and recorded on signal film using the ERIM/Seasat film recording system at the Applied Physics Laboratory (Shuchman, et al., 1978). This recording system has a nominal sweep speed of 500 m/sec and a film drive speed of 32.9 mm/sec; however, in order to determine these parameters more exactly, a set of measurements was made on the signal film itself.

To determine the recorder sweep speed, the pattern resulting from a 10 MHz test signal recorded on the signal film was examined. By counting cycles with a toolmaker's microscope, the spacing was found to be 5.40×10^{-5} m/cycle. Multiplying this by the frequency (10^7 cycles/sec), a sweep speed of 540 m/sec was obtained.

To determine the film drive speed, a calibrated grating with a line spacing nearly equal to that of the signal film was placed over the film, and the resulting Moire fringe pattern was observed. Using a grating with 49.98 cycles/mm, 8.5 cycles were observed over a

13.9 mm length of the Moire fringe pattern. Thus, the spatial frequency of the signal film is

$$F_s = 49.98 - \frac{8.5 \text{ cycles}}{13.9 \text{ mm}} = 49.37 \text{ cycles/mm} . \quad (1)$$

Dividing this into the pulse repetition frequency of 1646.75 Hz, the film drive speed was determined to be 33.36 mm/sec.

Once these recording system parameters are known, the scale factors of the signal film can be determined with information from the sensor data record. The azimuth scale factor can be calculated from the film speed if the swath velocity is known. This velocity was obtained from the sensor data record for each quarter-swath, as shown in Table 1. Using these values, the along-track scale factor of the signal film is 201,926 for swath 1, 201,920 for swath 2, and 201,915 for swath 3. Swath 4 was not processed during this experiment.

The slant range scale factor of the signal film is obtained from the sweep speed V_s using the equation

$$F_r = \frac{c}{2V_s} = \frac{2.998 \times 10^8 \text{ m/sec}}{2(540 \text{ m/sec})} = 277,600 . \quad (2)$$

The ground range scale factor is equal to the above divided by the sine of the incidence angle. Thus, at the center of swath 1 the ground range scale factor of the signal film is $277,600/\sin 20.698^\circ = 785,420$. Similarly, the ground range scale factors for swaths 2 and 3 are 726,000 and 676,480 respectively. Note that the ground range scale factor changes continuously across the swath so that at the edges of swath 1, for example, the scale factors are 819,630 and 754,130 (i.e., about ± 4 percent different from the scale factor at the center of the swath).

The scale factor of the image film is determined in the range direction by the processor range magnification, and in the azimuth direction by the ratio of the input film speed to the output

TABLE 1
SDR DATA FOR PORTION OF REV. 651 CONSIDERED

<u>Swath</u>	<u>Swath Velocity</u>	<u>Incidence Angle (at Near Range)</u>
1	6736.253 m/sec	19.797°
2	6736.061 m/sec	21.599°
3	6735.870 m/sec	23.365°
4	6735.680 m/sec	25.093°

film speed. The range magnification of the ERIM optical processor is 1.0044. Thus, to achieve unity aspect ratio at the center of swath 1, the film speed tracking ratio must be

$$R_t = \frac{785,420/1.0044}{201,926} = 3.873 \quad (3)$$

For swath 2, the tracking ratio is 3.580 and for swath 3 the tracking ratio is 3.335. Image films were generated for each of these swaths using these processor settings.

Finally, the image films were printed using the appropriate magnifications in the enlarger to obtain a nominal scale of 1:250,000. The appropriate magnification is the ratio of the image film scale to the desired print scale, i.e., 3.128 for swath 1, 2.891 for swath 2, and 2.694 for swath 3. An example of the imagery for swath 1 is shown in Figure 1.

2.2 EVALUATION

The actual scale of the output prints was evaluated by comparing them to 1:250,000 scale U.S. Army Corps of Engineers map number NJ16-6. Features along the Ohio River, which runs in approximately the range direction were located near the edges and center of each swath. The across-track scale factor was computed separately for each half of the swath by comparing the distances between features near the center and at the edges of the swath, and for the entire swath by comparing distances between features near opposite edges of the swath. The results are summarized in Table 2. Note that there is a consistent pattern of larger image scale factors for the left side of each swath than for the right side. This is in agreement with expectations since the ground range scale factor depends on the incidence angle and the processor was set up to yield unity aspect ratio at the center of each swath.

ORIGINAL PAGE IS
OF POOR QUALITY

Σ EF 1

RADAR AND OPTICS DIVISION

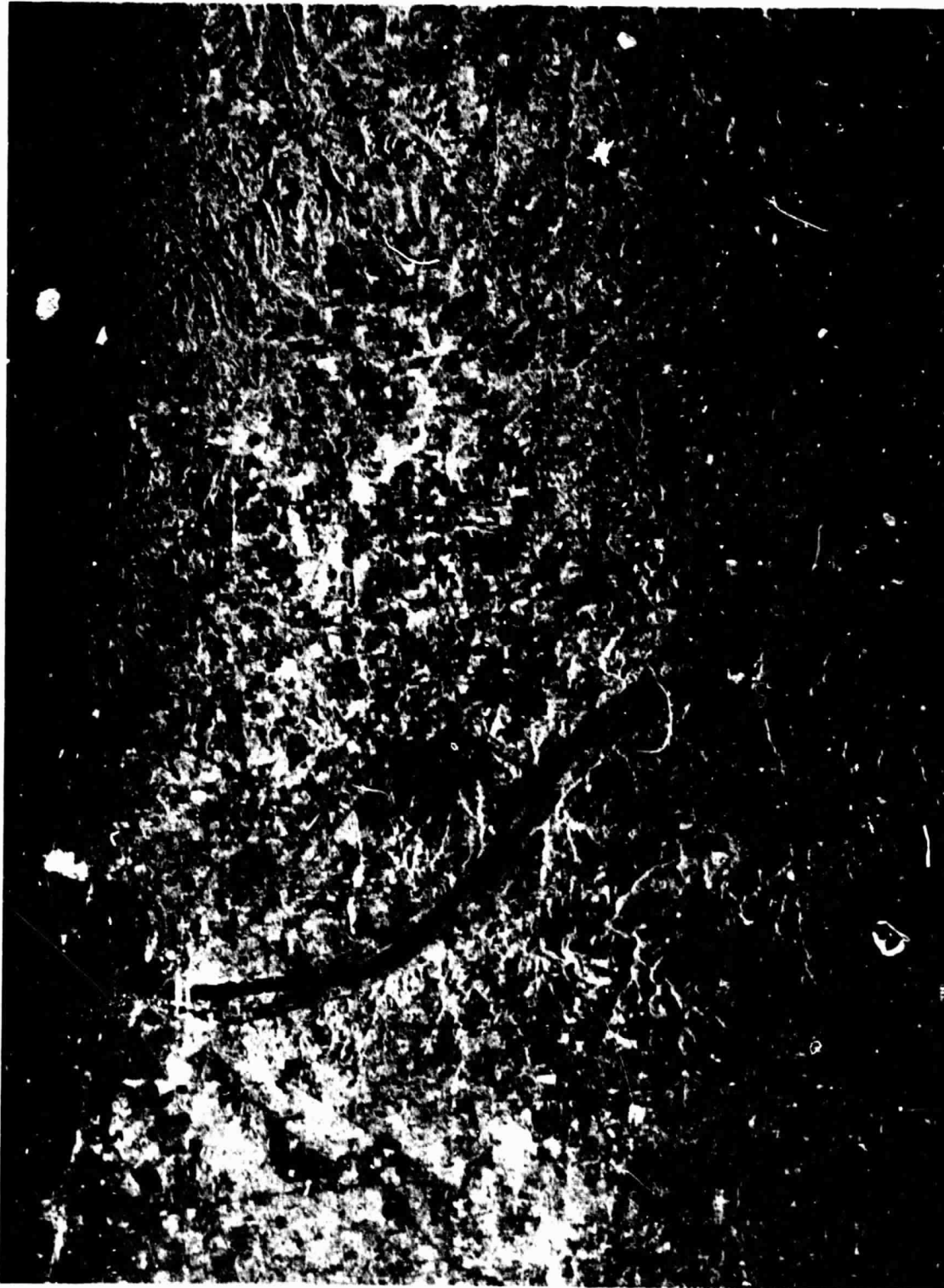


FIGURE 1. PORTION OF REV. 651 IMAGE USED FOR SCALE EVALUATION.

TABLE 2
OBSERVED DIFFERENCES IN ACROSS-TRACK SCALE FACTORS
BETWEEN SAR IMAGE AND MAP

<u>Swath</u>	<u>Left Side (%)</u>	<u>Right Side (%)</u>	<u>Entire Swath (%)</u>
1	+2.8	-3.3	-0.4
2	+0.8	-6.1	-2.7
3	-1.5	-5.7	-3.5

There also appears to be an overall decrease in the image scale factor from swath 1 to swath 3. The reason for this is not known but may be due to errors in the SDR incidence angle data, errors in processor settings, or inaccuracies in the scale factor measurements. The along-track scale factor was found to be accurate to within 0.3 percent of the map scale factor.

2.3 SUMMARY

This study was designed to test the accuracy with which a specified image scale factor could be obtained in optically processed Seasat imagery. The results indicate that by using only the system parameters given in the SDR, the properties of the film recording system, and the magnification settings of the optical processor, an image scale factor can be predicted to within ± 0.3 percent for the azimuth (along-track) direction.

In the range (across-track) direction, the image scale factor is observed to deviate by as much as 6 percent from the predicted value (see Table 2). A ± 4 percent deviation was expected for the data studied, assuming that the specified scale factor was produced at the center of the swath. Such deviations can be expected in any optically processed imagery because the processor cannot compensate for the decrease in the ground range scale factor due to incidence angle variations within each swath. The difference between the observed 6 percent deviation and the expected 4 percent deviation is apparently due to an overall decrease in the image scale factor from swath 1 to swath 3. This change may be due to errors in processor settings, interpretation of SDR incidence angle data, or to measurement inaccuracies.

3
IMAGE FILM RADIOMETRY

The microwave radiometric characteristics of objects resolved by a Synthetic Aperture Radar (SAR) may be observed in the output image of the SAR. Radar cross section measurements are usually made photometrically in the image plane of the optical processor. However, it is sometimes necessary to make radiometric measurements on the output imagery as recorded on film, for example where the investigator does not have access to an optical processor. This section of the report discusses the problems involved in extracting backscatter cross section values from SAR image films, and makes recommendations for improving this procedure.

3.1 BACKGROUND

The usual method of making cross section measurements in a SAR optical processor is to record the electrical current generated by a photomultiplier tube (PMT) intercepting the light flux passing through a suitable aperture in the image plane. When measuring the cross section of a point target, the aperture is chosen to pass only the light in the point image. Measurements of average reflectivity for distributed targets are made by adjusting the aperture to pass the flux representing the area to be averaged. If the scale of the image plane is known, the aperture size in radar space may be determined and measurements of reflectivity per unit area can be computed. Absolute measurements may be inferred if objects of known cross section, such as calibrated corner reflectors, are included in the image.

When the image produced by the SAR optical processor is recorded on photographic film, the photometric properties of the image are transformed to density variations on the recording film. If the recording characteristics of the image film are precisely known, it is

possible to calculate the original photometric properties of the image and thus the radiometric properties of the imaged area. These characteristics can be established in part by a step wedge exposure on the image recording film. The additional information needed to obtain absolute radar cross section measurements from the image film is the film density for an object or area of known radar cross section. The calculation of radar cross sections for distributed targets is discussed in the following section. Additional considerations involved in the use of point targets, such as corner reflectors, for calibration are discussed in Section 3.3.

3.2 RADAR CROSS SECTION MEASUREMENTS

The relative radar reflectivity of two radar image areas may be defined as the ratio of the cross section per unit area (σ_0) for each location, i.e.,

$$\text{Backscatter Ratio} = \sigma_{02}/\sigma_{01} \quad (4)$$

where σ_{02} is the reflectivity of the test area, and σ_{01} is the reflectivity of a reference area.

The reflectivity of the terrain is related to the image intensity, radar calibration constant, and collection geometry by

$$\sigma_0 = IC \cos \phi \quad (5)$$

where I is the image intensity, C is the radar calibration factor, and ϕ is the depression angle.

The calibration factor C includes the effect of antenna gain and range to the target as well as other factors. It therefore generally varies over the radar image and must be taken into account when objects at different ranges and depression angles are compared. The cosine factor appears in the σ_0 expression because the SAR image

has coordinates corresponding to the slant range plane and σ_0 is defined in ground coordinates.

The reflectivity ratio may then be related to the image intensities as

$$\frac{\sigma_{02}}{\sigma_{01}} = \frac{I_2 C_2 \cos \phi_2}{I_1 C_1 \cos \phi_1} \quad (6)$$

When the image is recorded on film, the intensities I_1 and I_2 are converted to corresponding image densities D_1 and D_2 by action of the film exposure E and the photographic development of the film. By definition

$$E = It \quad (7)$$

where t is the effective exposure time of the recording process.

The usual way of relating the exposure and density characteristics of a film is by the D vs. $\log E$ curve. An example is shown in Figure 2.

When the density and \log exposure scales are equal, the slope of the straight line portion of the curve describes the contrast or "gamma" of the film; i.e., $\gamma = \tan \alpha$ where α is the angle of the straight line portion with respect to the horizontal axis. When D_1 and D_2 fall on the straight line portion of the D vs. $\log E$ curve, the image intensity ratio can be found by using the relationship developed below:

$$\begin{aligned} D_1 - D_2 &= \gamma [\log E_1 - \log E_2] \\ &= \gamma \log (E_1/E_2) \\ &= \gamma \log (I_1 t / I_2 t) \\ &= \gamma \log (I_1 / I_2). \end{aligned} \quad (8)$$

Then

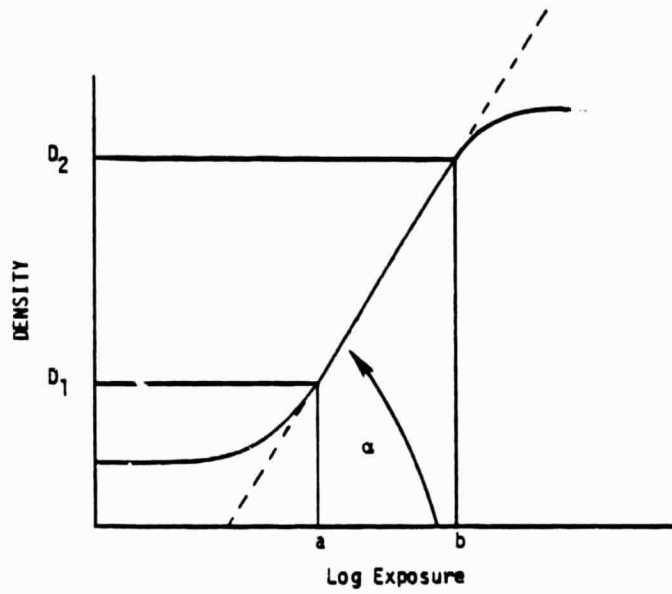


FIGURE 2. TYPICAL DENSITY VS. EXPOSURE PLOT FOR PHOTOGRAPHIC FILM.

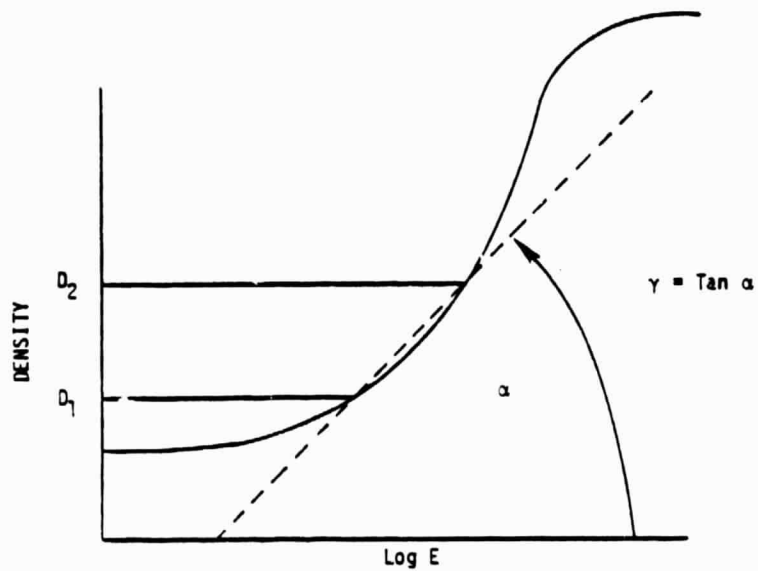


FIGURE 3. EFFECTIVE FILM "GAMMA" FOR POINTS NOT ON THE LINEAR PART OF THE CURVE.

$$(D_1 - D_2)/\gamma = \log (I_1/I_2). \quad (9)$$

This intensity ratio may then be related to the relative backscatter ratio σ_{02}/σ_{01} given in Eq. (6). The ratio in dB is given by

$$10 \log \frac{\sigma_{02}}{\sigma_{01}} = 10 \log \frac{I_2 C_2 \cos \phi_2}{I_1 C_1 \cos \phi_1}. \quad (10)$$

Substituting for the intensity ratio, the density relationship in Eq. (9), the backscatter ratio in dB is given by

$$10 \log \frac{\sigma_{02}}{\sigma_{01}} = 10 \log \frac{D_2 - D_1}{\gamma} + 10 \log \frac{C_2}{C_1} + 10 \log \frac{\cos \phi_2}{\cos \phi_1}. \quad (11)$$

For situations where the depression angle ϕ and the calibration constant C are essentially the same for the two areas to be compared, the backscatter ratio in dB is approximately

$$10 \log \frac{\sigma_{02}}{\sigma_{01}} = 10 \log \frac{D_2 - D_1}{\gamma}. \quad (12)$$

If the densities D_2 and D_1 are not on the straight line portion of the curve, the intensity ratio may still be found using the above relations if γ is computed as the slope of the line joining points D_2 and D_1 on the D vs. $\log E$ curve. This is shown graphically in Figure 3.

When the resulting value of γ is significantly different from that of the straight line portion of the D vs. $\log E$ curve, the accuracy of the ratio measurement will be reduced. For this reason the film recording exposure should be chosen to place the densities of all the areas of interest on the straight line portion of the D vs. $\log E$ curve if possible.

The absolute value for the cross section of a test area, σ_{02} , can be obtained only by making measurements relative to a reference

area with known radar cross section. Frequently, point targets such as corner reflectors are used for calibration. However, the measurement of peak density for such point objects on the image film is difficult because of the small size of the images and the lack of suitable instrumentation for making point density measurements. Microdensitometer scans may be used, but multiple scans must be made to be sure that the peak density is recorded. The densities produced by point image exposures may also have sensitometric characteristics that differ from those made from large area exposures such as produced by a standard step table. A measurement of this effect is described in Section 3.3. In addition, the reflector responses will often be saturated in images where the exposure level is chosen to record the average terrain at normal density levels. Because of the factors cited above it is extremely difficult if not impossible to calculate accurately the relative energy content of reflector responses by measuring their corresponding image densities. Fortunately, the measurement of average exposure levels for distributed radar returns usually relates directly to standard photographic sensitometer exposures, as shown in Section 3.4, and measurement of relative average backscatter may be readily made using standard photographic instrumentation. Absolute measurements of average backscatter are then possible if a reflectivity standard for the radar image, established by the usual photometric means in the optical processor, is recorded as part of the imagery package.

3.3 IMAGE POINT DENSITY MEASUREMENTS

Point density vs. exposure level measurements were made for Seasat corner reflector images of the Goldstone reflector array as recorded on signal film No. 286 of Rev. 882. The measurements were made using imagery recorded on Kodak 3414 film and a modified form of the Joyce-Lobel microdensitometer. The radar resolution was approximately 10 meters in azimuth by 25 meters in ground range.

The image scale was approximately 700,000:1 yielding an image film resolution of about 14 μm by 35 μm . It was not possible to make accurate peak density measurements of these small spots using the standard optical arrangement of the Joyce-Lobel microdensitometer because it was impossible to observe the alignment of the spot image at the aperture screen. To circumvent the problem, the image was projected with approximately a 10-X magnification into a 50 μm Gamma Scientific photometer probe by means of a mirror, using the illumination source and scanning table of the Joyce-Lobel instrument. The scanning table of the microdensitometer was used to position the film so that the point images were properly aligned with the 50 μm probe. Densities (D) were then calculated by recording the light level indicated on the Gamma Scientific autophotometer and then using the relation

$$D = \log (B/P) \quad (13)$$

where B is the background reading with film removed, and P is the minimum light reading through the reflector image.

The point density vs. exposure characteristic was established by generating a sequence of images on the ERIM precision optical processor using 3 dB light level increments. A standard sensitometer exposure was included to establish the D vs. E characteristic for the film.

The light level measurements used to compute the image densities are shown in Table 3. The measurements were made difficult by the presence of a granular "anti-stick" coating on the back of the film. The random orientation of the relatively large grains lead to a differential refraction of the light beam away from the measurement path. Consistent density measurements were possible only after the back side of the 3414 film was covered with immersion oil and a glass plate.

TABLE 3
 CORNER REFLECTOR IMAGE DENSITY MEASUREMENTS
 Background Measurement B = 20 (In Same Units As P, Below)

<u>Exposure</u>	<u>Reflector 1</u>		<u>Reflector 2</u>	
	<u>P</u>	<u>D</u>	<u>P</u>	<u>D</u>
0	52.0	0.32	98.0	0.09
+3 dB	20.0	0.78	45.0	0.43
+6 dB	4.4	1.44	14.0	0.93
+9 dB	0.96	2.10	2.3	1.71
+12 dB	0.42	2.46	0.58	2.32
+15 dB	0.32	2.57	0.36	2.52

The point densities calculated above are plotted in D vs. $\log E$ format in Figure 4. The standard sensitometer densities as measured with the McBeth densitometer are plotted on the same graph. The slope of the D vs. $\log E$ curve for the two point image responses is approximately 2.2 as shown on the graph. This is significantly higher than the 1.55 slope of the standard sensitometry curve. Additional step wedge density measurements were made using the point density instrumentation. The slope of the resulting curve as shown in Figure 4 was slightly higher than that for the McBeth measurements, but still much lower than that of the point measurements.

The reason for this difference is not known, but may be due to adjacency effects in the film development process. These effects are caused by differing rates of depletion of the developer for point images and diffuse images.

3.3 DISTRIBUTED REFLECTANCE MEASUREMENTS

In this part of the study, measurements were made of the image film density for a uniformly reflecting area as a function of the exposure level. This was done to confirm that the sensitometric properties of the film were the same for such distributed reflectors as for the standard sensitometer exposures. A simulated signal film, consisting of a Mylar diffuser, was used in the optical processor. The processor bandwidths were set up for Seasat processing and an image film was exposed using various laser illumination levels. Prior to development of this film, a standard set of sensitometer exposures was also added to the film.

After development, the density of the sensitometer step wedges was measured and plotted versus the exposure. The density of the simulated images was also measured and plotted versus the laser illumination level. The resulting plots, shown in Figure 5, indicated similar characteristics (i.e., γ) for the step wedges and the test

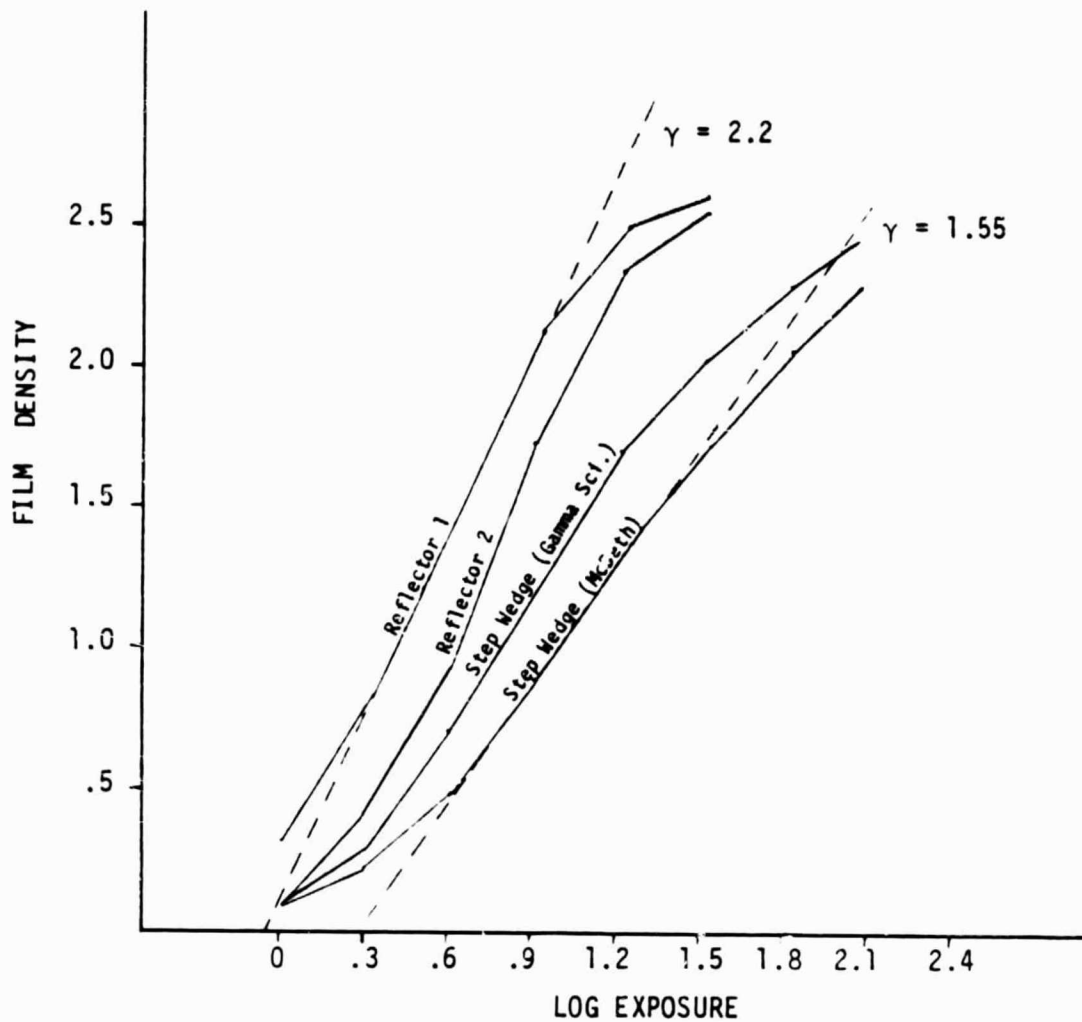


FIGURE 4. RESPONSE CURVES FOR POINT TARGETS AND STEP WEDGES USING KODAK 3414 FILM.

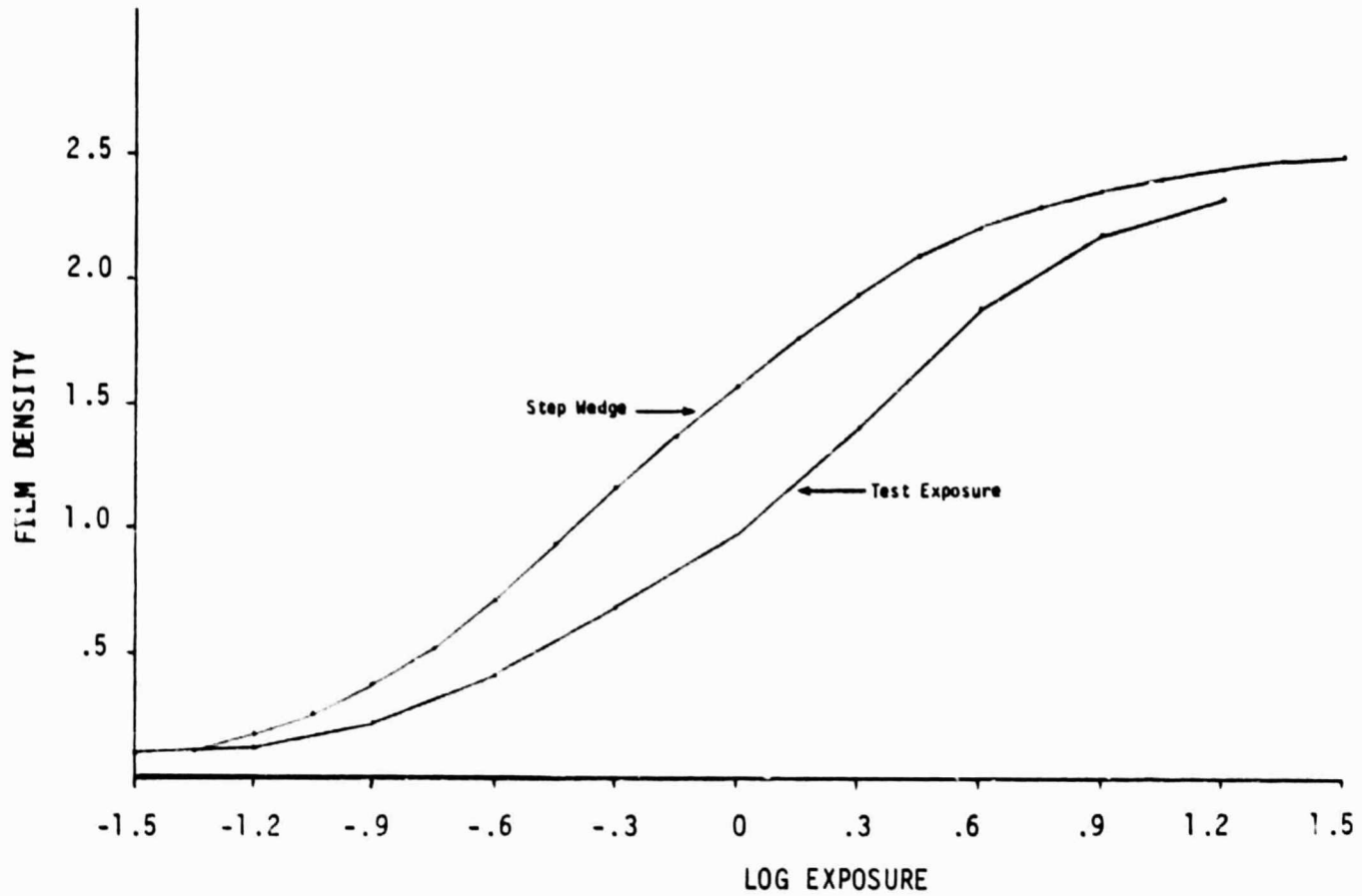


FIGURE 5. FILM CHARACTERISTICS FOR DISTRIBUTED TARGETS.

exposures. Thus it appears to be valid to apply standard sensitometric techniques to distributed targets in SAR imagery.

3.4 SUMMARY AND RECOMMENDATIONS

The conclusion which follows from these measurements is that it is not feasible to use point targets, such as corner reflectors, to calibrate the image film for distributed targets since the film response is different for point targets and distributed targets. One possible solution of this problem is to make measurements of the point target response in the optical processor and use these measurements to infer the cross section per unit area, σ_0 , of a uniform area in the scene. Since distributed targets do appear to have the same densitometric properties as the standard sensitometer exposures, a uniform area of known σ_0 could then serve as a secondary calibration reference for the image film.

The accuracy of both relative and absolute backscatter measurements is generally reduced as the time between data collections for the two areas to be compared increases. Even during a single data pass the radar calibration factor C (Eq. (5)) may vary for identical radar ranges as a result of combinations of the following:

1. Receiver gain changes
2. Transmitter power variations
3. Signal film density variations
4. Azimuth (Doppler) spectrum wander due to antenna orientation changes and electronic offset errors
5. Antenna gain variations due to radar platform roll.

If the effects of these variations are not properly accounted for, serious backscatter measurement errors will result. In particular, failure of the radar motion compensation system to adequately control azimuth spectrum wander often produces "banded" imagery with gross

changes of image intensity over relatively short along-track distances. Seasat radar data are also affected by Doppler spectrum shifts due to earth rotation effects as described in the following chapter of this report. Accurate backscatter calculations may be made under the above conditions if their effect on the value of the calibration constant are precisely known. If they are unknown, backscatter measurements will be equally uncertain.

RADIOMETRIC EFFECTS OF DOPPLER SPECTRUM VARIATIONS

The along-track radiometric stability of the Seasat SAR is an issue of concern to those attempting to correlate the SAR image intensity with geophysical parameters, such as winds, over large areas. The study reported in this section deals with one aspect of this problem, namely the effect of Doppler spectrum variations on the radiometric properties of the SAR image. The discussion is in the context of optically processed imagery since the ability of optical methods to process long swaths in a continuous manner makes these methods attractive for this application. The effects of Doppler spectrum "wandering" on digitally processed data must also be considered when comparing successive frames of imagery, but these effects are beyond the scope of the present study.

4.1 BACKGROUND

The azimuth, or Doppler, spectrum of the signals received by a SAR is dependent on the antenna gain pattern, the antenna look direction, the platform velocity, and the radial velocity of the objects in the scene. For Seasat, the received Doppler spectrum has a width of about 900 Hz. Because this spectrum is, in effect, sampled at the pulse repetition frequency (PRF) the actual spectrum is not distinguishable from a set of "alias" spectra separated in frequency by multiples of the PRF. Approximating the antenna gain pattern by a Gaussian function, the received signal spectrum can be written as

$$S_i(f) = \sigma_0 \sum_{n=-\infty}^{\infty} \exp\left\{-2.77 \left(\frac{f - f_c - nf_r}{B}\right)^2\right\} \quad (14)$$

where σ_0 is the radar cross section of the surface, $B = 900$ Hz is the 3 dB bandwidth of the Doppler spectrum, f_c is the peak frequency, and $f_r = 1647$ Hz is the pulse repetition frequency (PRF).

When this signal is recorded on film, the higher frequencies are attenuated, or recorded with less efficiency than the lower frequencies. This effect is described by the modulation transfer function (MTF) of the recording system. Measurements in the optical processor indicate that the shape of the MTF can be approximated by the sum of a Gaussian and an exponential function, i.e.,

$$M(f) = \frac{1}{2} e^{-\left(\frac{f}{B_r}\right)^2} + \frac{1}{2} e^{-\left|\frac{f}{B_r}\right|} \quad (15)$$

where $B_r = 600$ Hz is the recording system bandwidth. Thus, the spectrum of the signals recorded on the signal film (as measured in the optical processor) is given by

$$S_o(f) = M(f)S_i(f) + N(f) \quad (16)$$

where $N(f)$ is the noise spectrum, which has approximately the same shape as the MTF. Examples of measured spectra for Seasat Rev. 757 are shown in Figures 6-10. Note that the effects of the MTF are clearly visible in these measurements, causing the alias spectra to be of unequal amplitude and the peak frequencies to be separated by less than the PRF. Note also that the peak frequencies vary as a function of the distance along the swath during this pass. The implications of this spectrum shift for the radiometric calibration of the data will be discussed in Section 4.3.

4.2 DOPPLER SPECTRUM MEASUREMENTS

In order to measure the spectral shifts during Rev. 757, the spectra shown in Figures 6-10 were divided by the MTF. Using the measured MTF, the data appeared to be over-corrected, as indicated by the amplitudes and separation of the real and alias spectra. Using a modified MTF of the same form as Eq. (15) but with $B_r = 900$ Hz, a better correction was obtained. The corrected spectra

FIGURE 6. AREA A

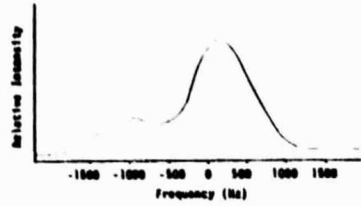


FIGURE 7. AREA B

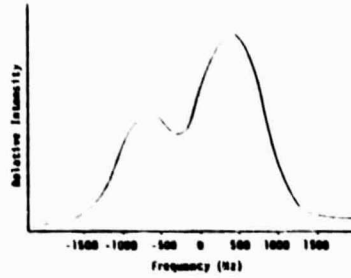


FIGURE 8. AREA C

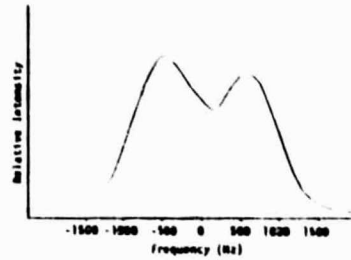


FIGURE 9. AREA D

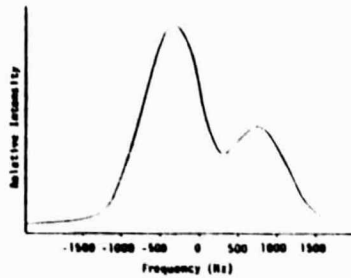
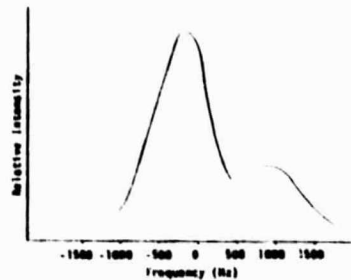


FIGURE 10. AREA E



MEASURED DOPPLER SPECTRUM

using this MTF are shown in Figures 11-15, and the peak frequencies of the real and alias spectra are shown in Table 4.

Shifts in the peak frequency of the Doppler spectrum along the swath are due to earth rotation effects and spacecraft attitude variations. The Doppler shift due to the earth's rotation is given by

$$\Delta f_c = - \frac{2 \Omega R_e}{\lambda} \cos (L) \sin \phi \sin \theta \quad (17)$$

where Ω is the earth's angular velocity (7.272×10^{-5} rad/s), R_e is the earth's radius (~ 6370 km), λ is the radar wavelength (23.5 cm), L is the latitude, ϕ is the radar look direction (from North), and θ is the incidence angle ($\sim 20^\circ$).

The Doppler shift due to spacecraft attitude variations is given approximately by

$$\Delta f_c = \frac{2V}{\lambda} (\cos \theta \sin P - \sin \theta \sin Y) \quad (18)$$

where V is the swath velocity (nominally 6800 m/s), P is the pitch angle, and Y is the yaw angle. P is positive for nose-up rotations of the spacecraft and Y is positive for clockwise rotations (looking down). These angles are given in the auxiliary data listing for the Seasat pass under consideration.

The latitude variation and changes in pitch and yaw for a portion of Rev. 757 are shown in Figure 16. Also shown in this figure are the calculated Doppler shifts due to the earth's rotation and the changes in spacecraft attitude along the pass. The total Doppler shift is shown in Figure 17, along with the peak frequencies obtained from the optical processor measurements. Note that the trend is predicted quite well by the above equations. There is an offset of about 200 Hz between the calculated and observed Doppler frequencies, but this is to be expected since there are Doppler shifts introduced during the transmission and recording of the data which are not accounted for in these calculations.

INPUT SIGNAL - 20 m from end

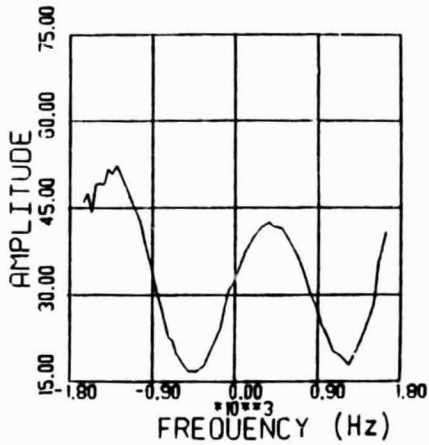


FIGURE 11. CORRECTED DOPPLER
SPECTRUM FOR AREA
A, REV. 757.

INPUT SIGNAL - 15 m from end

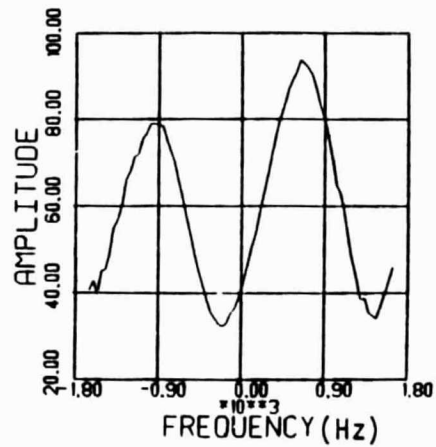


FIGURE 12. CORRECTED DOPPLER
SPECTRUM FOR AREA
B, REV. 757.

INPUT SIGNAL - 10 m from end

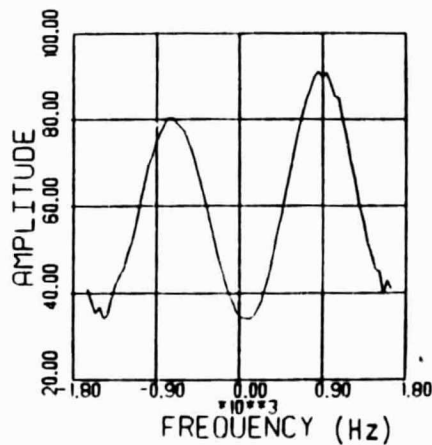


FIGURE 13. CORRECTED DOPPLER
SPECTRUM FOR AREA
C, REV. 757.

INPUT SIGNAL - 5 m from end

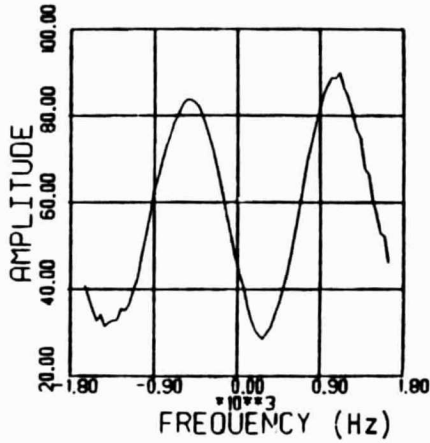


FIGURE 14. CORRECTED DOPPLER SPECTRUM FOR AREA D, REV. 757.

INPUT SIGNAL - end of pass

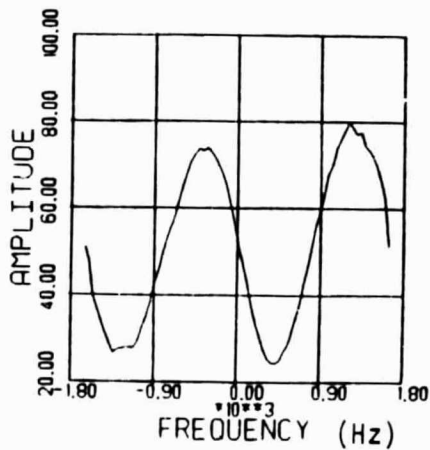


FIGURE 15. CORRECTED DOPPLER SPECTRUM FOR AREA E, REV. 757.

ORIGINAL PAGE IS
OF POOR QUALITY



RADAR AND OPTICS DIVISION

TABLE 4
DOPPLER PEAK FREQUENCIES MEASURED FOR REV. 757

<u>Location</u>	<u>Time</u>	<u>f_c (actual spectrum)</u>	<u>f_c (alias spectrum)</u>
A	22:37:36	400 Hz	-1300 Hz
B	22:40:13	700 Hz	-950 Hz
C	22:42:49	900 Hz	-730 Hz
D	22:45:25	1050 Hz	-500 Hz
E	22:48:01	1250 Hz	-400 Hz

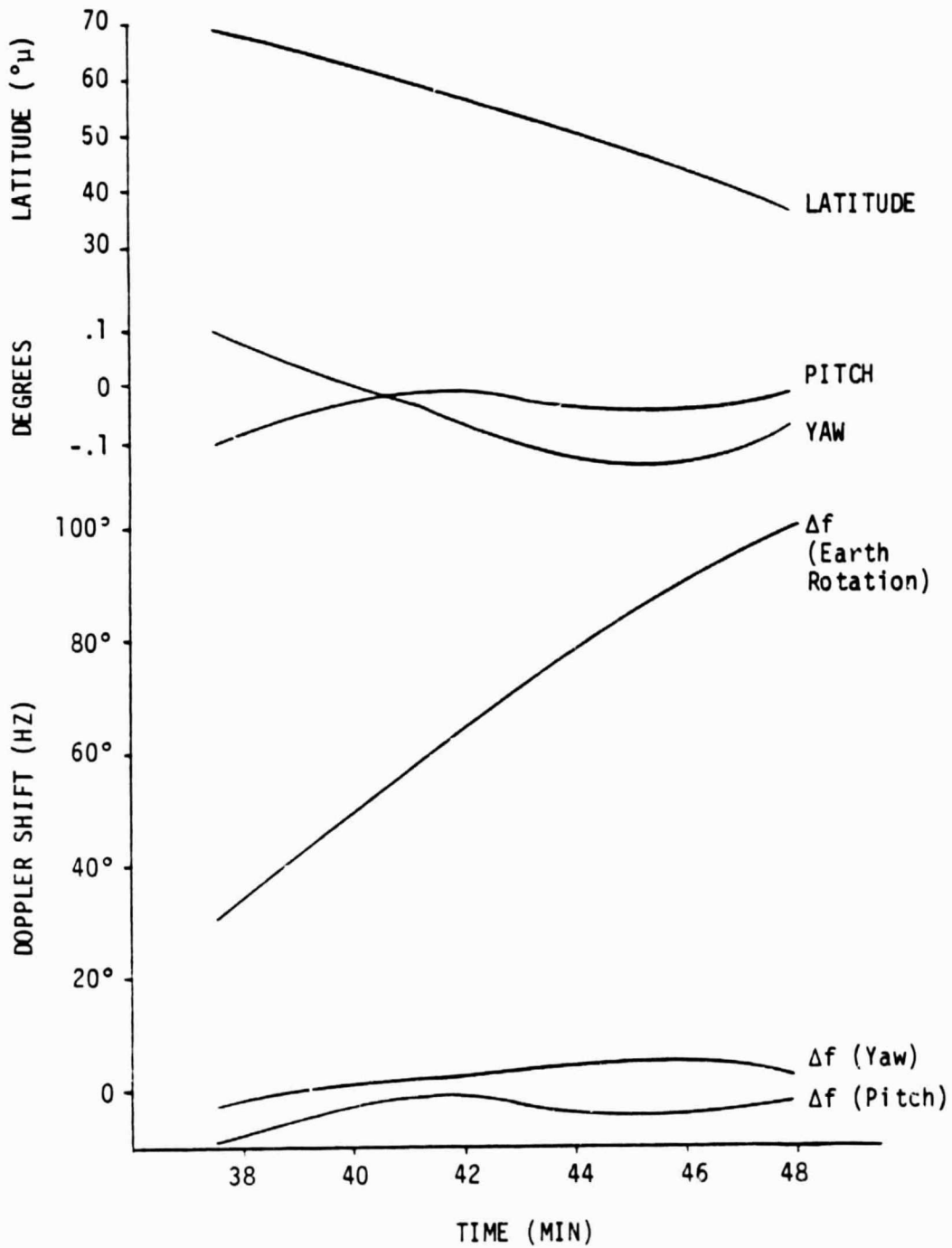


FIGURE 16. SEASAT ORBITAL PARAMETERS AND ASSOCIATED DOPPLER SHIFTS FOR REV. 757.

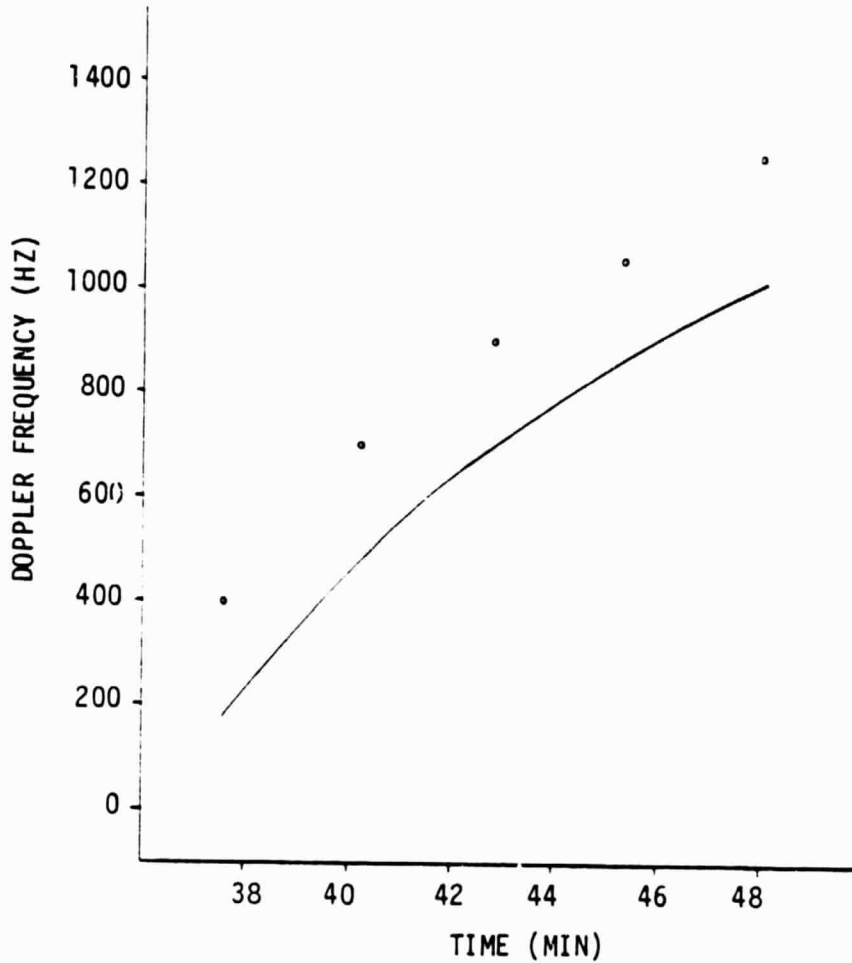


FIGURE 17. CALCULATED DOPPLER SHIFTS (SOLID LINE) DUE TO EARTH ROTATION AND SPACECRAFT ATTITUDE CHANGES, AND OBSERVED PEAK FREQUENCIES (CIRCLES) FOR SEASAT REV. 757.

4.3 RADIOMETRIC EFFECTS

The effects of changes in the Doppler frequency on the radiometric calibration of the data depend on how the data are processed. Normally, an aperture is placed in the frequency plane of the processor to block out the alias spectrum, in order to avoid azimuth ambiguities in the image. If this is done, the effective gain of the system will vary significantly along the swath, even if the location of the aperture is moved so as to track the changes in the spectrum location. This effective gain, defined as the ratio of the output power to the input power within the frequency aperture, is plotted versus the peak Doppler frequency in Figure 18 for an aperture width of 900 Hz centered about the peak frequency. The same gain factor is plotted versus time for Rev. 757 in Figure 17. It is apparent that this is a very significant effect which should be accounted for if the image intensity, or image film density, is used to infer the radar cross section of the surface over a long swath.

The radiometric effects of Doppler shifts are much less pronounced if measurements are made in the frequency plane of the processor using a wide enough aperture to pass both the primary and one alias spectrum, since a decrease in the amplitude of one peak is accompanied by an increase in the amplitude of the other. Note that this method effectively bypasses the image formation process and thus results in a much lower spatial resolution. There is still a slight variation in the effective gain of the system using this method, as shown in Figures 20 and 21, but the variation is small compared to other sources of error.

An alternative to this procedure would be to make explicit corrections for Doppler spectrum variations. This could be done by measuring the peak Doppler frequency at several points along the pass and calculating the gain as was done here. Such a correction would be especially important for measurements made on conventionally processed image films over large swath lengths.

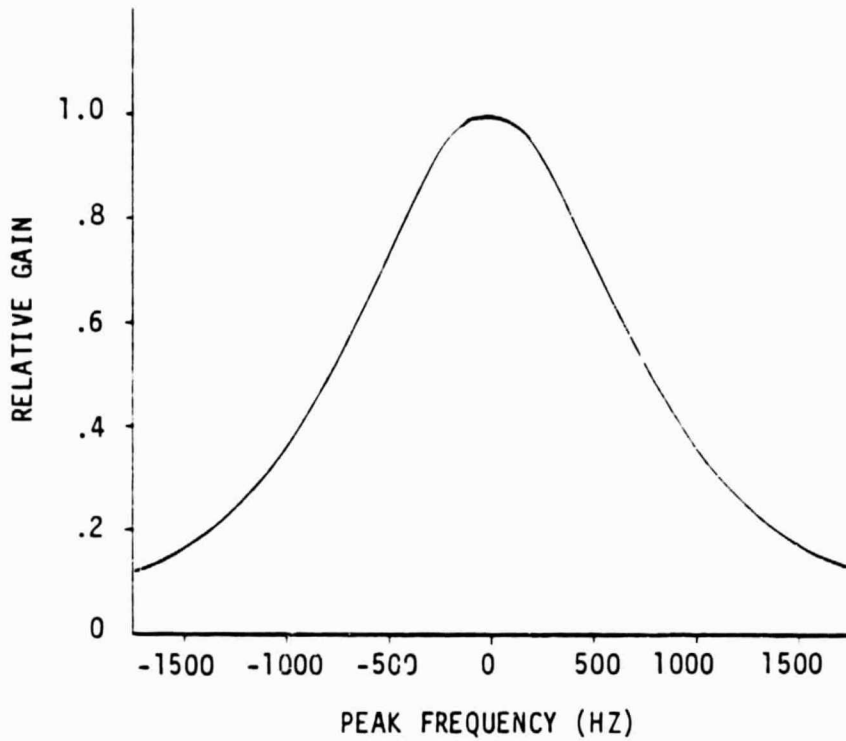


FIGURE 18. RATIO OF OUTPUT TO INPUT POWER WITHIN A FREQUENCY INTERVAL OF 900 HZ CENTERED AT THE DOPPLER PEAK FREQUENCY.

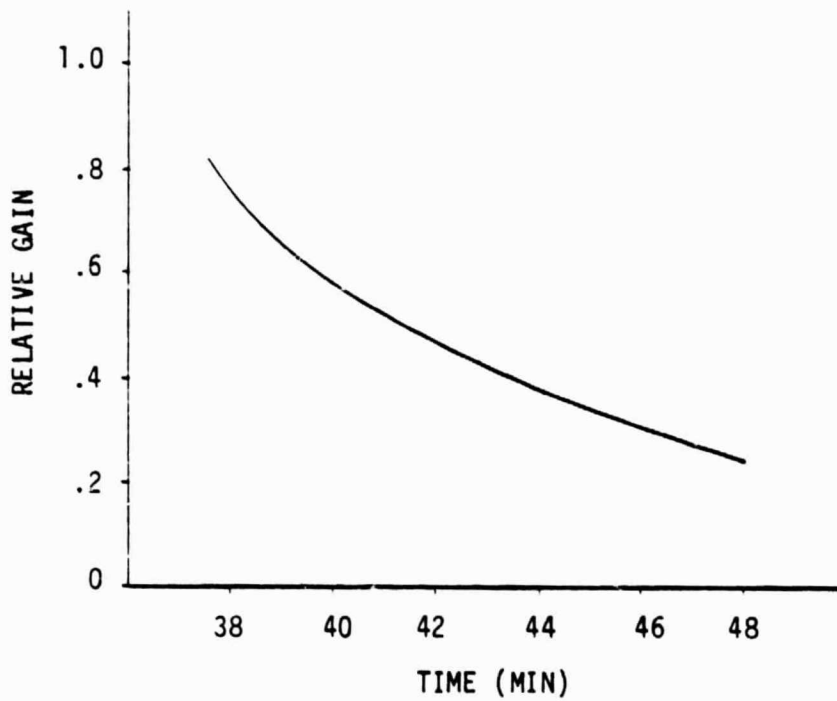


FIGURE 19. RATIO OF OUTPUT TO INPUT POWER FOR A SEGMENT OF REV. 757, USING A FREQUENCY-PLANE APERTURE OF 900HZ WIDTH CENTERED AT THE ACTUAL DOPPLER PEAK FREQUENCY.

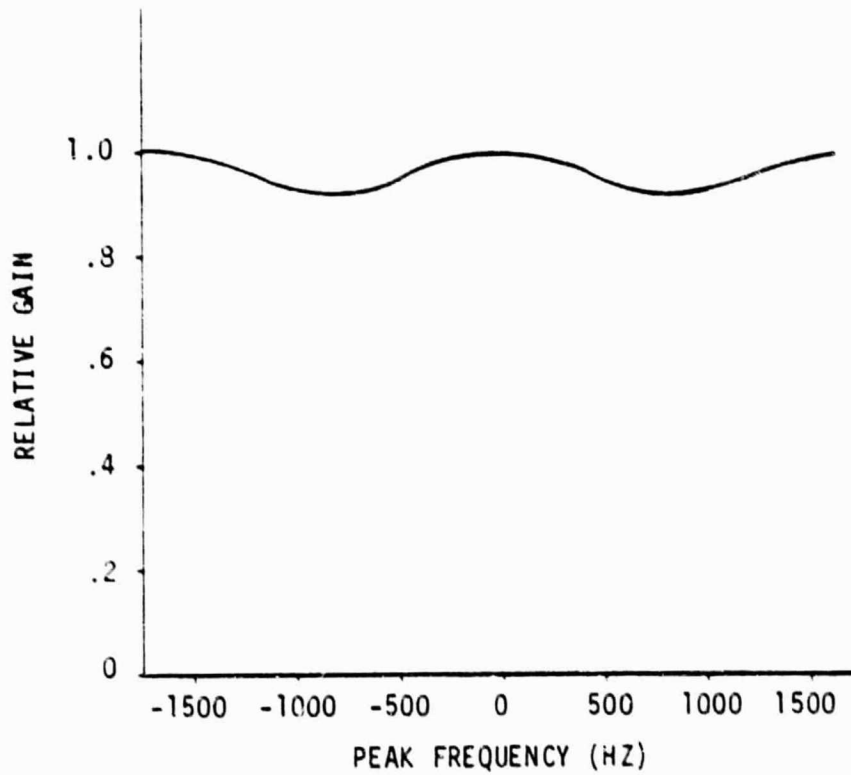


FIGURE 20. RATIO OF OUTPUT TO INPUT POWER FOR A FREQUENCY INTERVAL FROM -PRF TO +PRF VERSUS DOPPLER PEAK FREQUENCY.

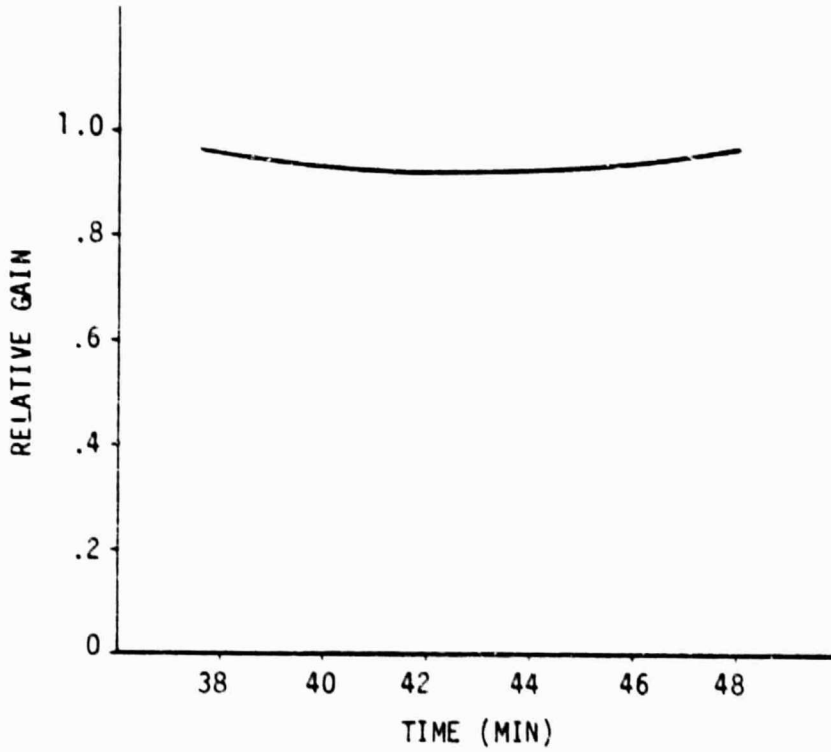


FIGURE 21. RATIO OF OUTPUT TO INPUT POWER FOR A SEGMENT OF REV. 757, USING A FREQUENCY-PLANE APERTURE FROM -PRF TO +PRF.

4.4 SUMMARY

Using optical processing techniques, variations in the Doppler spectrum of the received signal are observed to significantly affect the radiometric characteristics of Seasat SAR image data. These effects are sufficiently important that they should be accounted for if the image intensity is to be used to infer radar cross section over a long image swath, as, for example, in the measurement of surface wind speeds. It is found that these effects are much less pronounced if measurements are made in the frequency plane of the processor using an aperture which is wide enough to pass both the primary and one alias spectrum. These effects can also be corrected by determining a calibration curve of the effective gain for the pass from measurements of the peak Doppler frequency as a function of time. This correction method is especially applicable to intensity measurements made on conventionally processed image films over large swath lengths. Determination of proper MTF is important in the latter correction method, but is not needed in the frequency plane method.

REFERENCES

1. Shuchman, R.A., R.B. Innes, C.L. Liskow, B.T. Larrowe, and A. Klooster, ERIM Seasat SAR Engineering Evaluation, ERIM Report No. EM-79-1024, December 1978.
2. Shuchman, R.A., A. Klooster, J.D. Lyden, and C.L. Liskow, Engineering Evaluation of ERIM-Generated Seasat SAR Data, ERIM Report No. 151400-1-I, February 1981.

PRECEDING PAGE BLANK NOT FILMED